

# Motion estimation of tagged cardiac magnetic resonance images using variational techniques

N. Carranza-Herrezuelo<sup>a,\*</sup>, A. Bajo<sup>b,c</sup>, F. Sroubek<sup>d</sup>, C. Santamarta<sup>e</sup>, G. Cristobal<sup>a</sup>,  
A. Santos<sup>b,c</sup>, M.J. Ledesma-Carbayo<sup>b,c</sup>

<sup>a</sup> Instituto de Optica (CSIC), Serrano 121, Madrid Spain

<sup>b</sup> Biomedical Image Technologies. ETSI Telecomunicación. Universidad Politécnica de Madrid. 28040 Madrid, Spain

<sup>c</sup> Centro de Investigación Biomédica en Red en Bioingeniería, Biomateriales y Nanomedicina (CIBER-BBN), Spain

<sup>d</sup> Institute of Information Theory and Automation, Academy of Sciences of the Czech Republic, Pod vodárenskou věží 4, 182 08, Prague 8, Czech Republic

<sup>e</sup> Departamento de Física Matemática y Fluidos (Universidad Nacional de Educación a Distancia), Madrid Spain

## ARTICLE INFO

### Article history:

Received 26 March 2009

Received in revised form 20 January 2010

Accepted 18 March 2010

### Keywords:

Medical imaging processing

Motion estimation

Variational techniques

Tagged cardiac magnetic resonance images

Optical flow

## ABSTRACT

This work presents a new method for motion estimation of tagged cardiac magnetic resonance sequences based on variational techniques. The variational method has been improved by adding a new term in the optical flow equation that incorporates tracking points with high stability of phase. Results were obtained through simulated and real data, and were validated by manual tracking and with respect to a reference state-of-the-art method: harmonic phase imaging (HARP). The error, measured in pixels per frame, obtained with the proposed variational method is one order of magnitude smaller than the one achieved by the reference method, and it requires a lower computational cost.

© 2010 Elsevier Ltd. All rights reserved.

## 1. Introduction

The estimation of cardiac tissue motion and its deformation has been an area of major interest in medical image analysis [1]. Myocardial ischemia is a frequently encountered pathological problem that is caused by a locally reduced blood flow due to obstruction of the coronary arteries. The mechanical properties of an ischemic myocardium are altered, and therefore the injured tissue contracts irregularly. Non-invasive estimation of myocardial contractility is of great interest in order to detect regions with abnormal contraction. The degree of abnormality is also of importance to determine the potential of the injured region to recover contractile function after therapy [2].

The most important parameter to assess the regional function of the myocardium is the regional strain [3,4]. However, the myocardial strain measurement implies the accurate evaluation of the myocardial displacement.

Cardiac magnetic resonance (CMR) is one of the reference methods to perform the dynamic exploration of the cardiac function non-invasively. This imaging method is not only used to study the motion of the myocardial wall but also other functional parameters

such as perfusion and viability. Therefore, it is a very valuable imaging technique to assess the diagnostics of different cardiovascular diseases [5].

Cardiac motion assessment using conventional dynamic CMR imaging has recently been gaining more and more interest, primarily due to its availability and easier clinical application [6]. However, the main drawback of this imaging modality is the absence of reliable identifiable landmarks within the heart wall, which limits the assessment of the intramural motion [7,8]. Different magnetic resonance imaging (MRI) techniques have been proposed to overcome this problem: (1) Tagged MRI (TMRI); (2) Phase contrast magnetic resonance imaging (PCMRI); and (3) pulse field gradient-based MRI methods (Harmonic phase imaging (HARP)) and displacement encoding with stimulated echoes (DENSE [9]). TMRI modulates the underlying image intensity with the help of a specific pre-saturation technique [10]. This essentially produces a pattern of dark lines, or so-called *tags*, on the image. Deformation of these temporary lines is analyzed to derive a motion model of the underlying tissue. In contrast, PCMRI uses phase shifts induced in the transverse magnetization with "instantaneous" velocity-encoding pulses for measuring motion; the phase of the signal is directly related to the velocity of the material within each voxel at the time of velocity-encoding. The velocity field can then be integrated to get the displacement. In DENSE and HARP, a uniform pattern of phase modulation is encoded into the tissue at a chosen time, and the

\* Corresponding author. Tel.: +34 91 561 6800; fax: +34 91 564 5557.  
E-mail address: noemi.csic@gmail.com (N. Carranza-Herrezuelo).

deformation of that pattern is detected at a later time and utilized to estimate the motion [11–13].

Over the past years, tagged MR imaging has become an established technique to estimate myocardial motion [14], being available in most clinical scanners. Some of the methods proposed in the literature for the estimation of displacement fields include tracking intensity spatial modulation on the magnitude images (using segmentation of minimum intensity lines, optical flow, registration), using B-spline models [9,15,16] or tracking the harmonic phase (HARP) [11,17].

Tracking intensity minima is normally based on the development of an intensity profile model of a grid line. It is time-dependent, and it usually depends on a user who manually starts to identify the location of the lines. The most probable location is searched, or segmentation procedures are used such as morphological operations to locate dark lines in the image [18], matched filters [19,20], Gabor filters [21,22], deformable grids [23,24] or manually identified points [25]. The advantage of the optical flow methods is that they provide a dense estimation of the motion field in two dimensions rather than just a sparse set of data, and they do not require segmentation. There have been several strategies to perform the tracking of lines of the myocardium using such techniques [26–28], some of them trying to suppress the effects of the tag fading [29,30] or using registration techniques [31]. On the other hand, the HARP technique uses harmonic phase tracking to track the phase of the tissue tagging pattern in “angle” images [10,14,32].

Although the use of the HARP technique is widely spread [33,34], it is not commonly used for obtaining dense motion fields because of the calculation time required and the vulnerability of the method in the presence of noise. On the other hand, optical flow techniques allow motion field estimation from image sequences with reasonable computation cost, and they provide valuable information to process video sequences.

Variational methods have recently been used and have evolved as a powerful tool to solve problems in the field of image sequence analysis [11], image restoration [35], sequence segmentation and super-resolution [36,37]. Concerning optical flow estimation, several reviews have been published [38,39] covering the differences among the main optical flow techniques. Performance studies have proven that the variational approach is among the best methods [38]. However, the variational methods have not been applied to the myocardial motion estimation problem as much as the registration or phase harmonic-based methods. One can refer to [30] as a reference where a variational technique for motion estimation in tagged magnetic resonance sequences was considered.

In this paper, we propose the use of variational optical flow techniques to estimate displacements fields from MR tagged images. Preliminary results were presented in [40], using the standard variational technique and applying it to myocardial segmentation. In this paper, the use of variational methods for myocardial motion estimation is presented and validated in synthetic and real sequences. More in detail, a variational method with a total variation (TV) term has been adopted. Optical flow is estimated without smoothing the solution and preserving discontinuities in the optical flow. The intrinsic feature of the tagged images phase is used to perform more accurate and robust tracking, incorporating into the approach the motion estimates of control points with high phase stability.

## 2. Materials and methods

Many experiments provide evidence for superior performance of the variational optical flow techniques [38]. The basis of these methods is the constancy of the intensity structures of local time-varying image regions under motion, at least for a short duration

[41]. The use of this method actually assumes intensity conservation between consecutive frames that can be admitted in the case of tagged MR image frames separated by short time intervals as compared with T1 recovery [31]. However, if required, the T1 signal modulation could also be included in the criterion [31].

Formally, if  $u(x_1, x_2, t)$  is the intensity of the pixel  $(x_1, x_2)$  at time  $t$ ,

$$u(x_1(t), x_2(t), t) = \text{const}, \forall t \quad (1)$$

Taking the derivative at  $t=0$  with respect to time yields,

$$v(x_1, x_2) \cdot \nabla u(x_1, x_2, t_0) + u_t(x_1, x_2, t_0) = 0 \quad (2)$$

where  $v=(v_1, v_2)$ ,  $u_t = du/dt$  and  $v_1 = \frac{\partial x_1}{\partial t}$  and  $v_2 = \frac{\partial x_2}{\partial t}$  are the velocity fields. Eq. (2) is known as the optical flow constraint equation. However, we have only one equation for two unknown components of the velocity. This is the basis of the well-known aperture problem. Because this problem is underdetermined (ill-posed), additional constraints are required. One of the most popular constraints is based on the use of second-order derivatives, by choosing a parametric model of velocity or by regularizing the velocity fields [11]. In our formulation, we follow the regularization approach.

### 2.1. Variational approach

Horn and Schunck in [41] were the first to propose the following regularization term (B) in Eq. (3),

$$\min_v \int_{\Omega} \underbrace{(v \cdot \nabla u + u_t)^2 dx}_A + \alpha^r \int_{\Omega} \underbrace{(\|\nabla u_1\|^2 + \|\nabla u_2\|^2) dx}_B \quad (3)$$

where  $\alpha^r$  is a constant and  $\|\cdot\|$  is the usual Euclidian norm. Nevertheless, this term (B) smoothes isotropically, and it does not take into account the optical flow discontinuities [42]. More robust norms have to be considered to cope with discontinuities, and the one chosen in our approach is the following

$$\int_{\Omega} \phi(\|\nabla v_1\|) dx + \int_{\Omega} \phi(\|\nabla v_2\|) dx \quad (4)$$

where functions  $\phi$  allow noise removal and edge preservation. Among the different  $\phi$  functions proposed in [43], in this paper  $\phi(t)=t$  has been implemented and therefore Eq. (4) corresponds to total variation (TV). Very good anisotropic denoising properties of the TV semi-norm are well-known [36]. Since TV is highly nonlinear and non-continuous, special attention must be paid to its discretization. Several relaxed linearization schemes have been proposed. We follow the half-quadratic regularization scheme in [44] that introduces an auxiliary variable.

Finally, by including the terms above referred and an extra term for quasi-homogeneous areas [11], the energy minimization equation that we propose is given by

$$\min_v \int_{\Omega} (v \cdot \nabla u + u_t)^2 dx + \alpha^r \int_{\Omega} \phi(\|\nabla v\|) dx + \alpha^c \int_{\Omega} c(x) \|v\|_2^2 dx \quad (5)$$

#### 2.1.1. Implementation

The solution to the energy minimization in Eq.(5) with respect to the velocity fields  $v_1$  and  $v_2$  is characterized by the Euler–Lagrange equation, which in the vector-matrix notation takes the form [40]

$$\begin{pmatrix} [U_{X_1} U_{X_1} + \alpha^r L_1(z) + \alpha^c c] & [U_{X_1} U_{X_2}] \\ [U_{X_1} U_{X_2}] & [U_{X_2} U_{X_2} + \alpha^r L_2(z) + \alpha^c c] \end{pmatrix} \begin{pmatrix} v_1 \\ v_2 \end{pmatrix} = - \begin{pmatrix} U_t U_{X_1} \\ U_t U_{X_2} \end{pmatrix} \quad (6)$$

Matrices  $L_1$  and  $L_2$  appear from discretization of the regularization term in Eq. (4) [37] and depend on  $z$ , which is the auxiliary variable introduced by the half-quadratic scheme that can be calculated as

$$z(x, y) = \frac{\phi'(|\nabla v(x, y)|)}{|\nabla v(x, y)|} \quad (7)$$

Matrices  $L_1(z)$  and  $L_2(z)$  are Toeplitz matrices, positive semidefinite constructed by  $z$ , and they perform shift-variant convolutions with  $z$ . To avoid division by zero,  $z$  is defined for the TV case as,

$$z(i \pm 1/2, j \pm 1/2) = \begin{cases} \frac{1}{|\nu(i \pm 1, j \pm 1) - \nu(i, j)|} & \text{if } |\nu(i \pm 1, j \pm 1) - \nu(i, j)| > \varepsilon \\ \frac{1}{\varepsilon} & \text{otherwise} \end{cases} \quad (8)$$

where  $\varepsilon$  is the relaxation parameter [36]. Note that in the relatively flat regions,  $|\nabla v(x)| \leq \varepsilon$ ,  $L(z)$  becomes the Laplacian operator. In regions with a high image gradient,  $|\nabla v(x)| \geq \varepsilon$ ,  $\nu^T L(z) \nu$  approximates the TV semi-norm of the velocity  $\nu$ .

## 2.2. Enhanced method for tagged MR

In the same way that the homogeneous term has been added, it is easy to add other terms to adapt the algorithm to the problem. The main idea of the improved version has been introducing a regularization term in order to find a more accurate optical flow based on prior robust estimates in given control points. The new term is going to have information regarding the displacement of several points inside the myocardium with a very low error, and these points will henceforth be called control points. The term has the following form,

$$\beta \sum_i (v_i - p_i) \quad (9)$$

where  $p_i$  is the set of control points. The parameter  $\beta$  is a parameter determining the influence of Eq. (9) in the energy minimization Eq. (5).

With this equation, a solution of compromise is going to be obtained. The regularization term is going to provide a more accurate optical flow in the neighborhood of the control points. In those regions without any control point, this term does not have any effect.

Following the form of Eq. (6), the implementation equation that includes the new term is

$$\begin{pmatrix} [U_{X1}U_{X1} + \alpha^r L_1 + \alpha^c c + \beta M] & [U_{X1}U_{X2}] \\ [U_{X1}U_{X2}] & [U_{X2}U_{X2} + \alpha^r L_2 + \alpha^c c + \beta M] \end{pmatrix} \begin{pmatrix} v_1 \\ v_2 \end{pmatrix} = - \begin{pmatrix} U_r U_{X1} + \beta \cdot p_1 \\ U_r U_{X2} + \beta \cdot p_2 \end{pmatrix} \quad (10)$$

where  $M$  is a diagonal matrix with ones on positions corresponding to control points in Eq. (9).

Thus, the half-quadratic algorithm consists of the following steps:  $L_1$  and  $L_2$  are first initialized by velocities from a previous step (direct solution of optical flow equation). Then, new velocities are computed by solving Eq. (10).  $L_1$  and  $L_2$  are updated and Eq. (10) is solved again. The process is repeated until classical convergence criteria are met, such as the relative norm of differences or gradient are below a certain threshold. Empirically we have determined that for our synthetic and real data, five iterations were enough to achieve sufficient accuracy and keeping the computational cost low.

### 2.2.1. Obtaining the control points

Although Eq. (10) seems to have an easy implementation, obtaining the control points is a difficult task. Nevertheless, the tags of the image are an essential property that will allow such points to be obtained. There are some papers proposing tracking of the dark lines to find points of minimum intensity [17–20]. In this case, several points could be chosen between the tag lines as control points. Nevertheless, the tag fading is a limitation for these techniques, as the error allowed in the displacement estimation of those points has to be very small.

In contrast, techniques using the phase of the images (for instance, the HARP technique reported in [10,14]) turn out to be very accurate for tracking a few sets of selected points that have phases not affected by noise and where tag jumping is avoided. As we only need a set of points and not a dense optical flow for these control points, the control points will be a set of points with high stability of phase.

In 1-1 SPAMM (spatial modulation of magnetization) tagging pulse sequences [46–48], tags are created with a sinusoidal cross-sectional intensity profile. At any point on or between the tags, the tissue has both a magnetization intensity and a spatial phase of the periodic tag magnetization pattern, which are dependent on position [8]. Therefore, when the heart moves, a particular piece of tissue has the same phase in the deformed state as it has in the reference state. The phase of those images is an intrinsic property that can be tracked.

The control points are selected automatically taking into account that the phase of the tagged images is restricted to be in the range  $[-\pi, +\pi]$ . First the algorithm selects all the pixels belonging to a given range of phase in the phase image (in our case we selected from 0.4 to 0.5 rad which corresponds to the decay of the tag towards the trough). Following the previous process several pixels are selected in the same tag, therefore the algorithm further selects only those points belonging to tag intersections. Thus, a grid of selected points in the myocardium is formed (see Fig. 1). For tracking those points, a similar procedure to that reported in [8,10] is established using the Newton–Raphson method. The Newton–Raphson method is a well-known technique to find the root of a function. We applied it to a small region centered at the point of interest to find the roots in the difference of phase images. To avoid tag jumping, the Newton–Raphson method was only run in a small window around each point, taking into account tag spacing. Additionally, those points which had a difference of phase error higher than  $10^{-3}$  were rejected. Therefore, only points

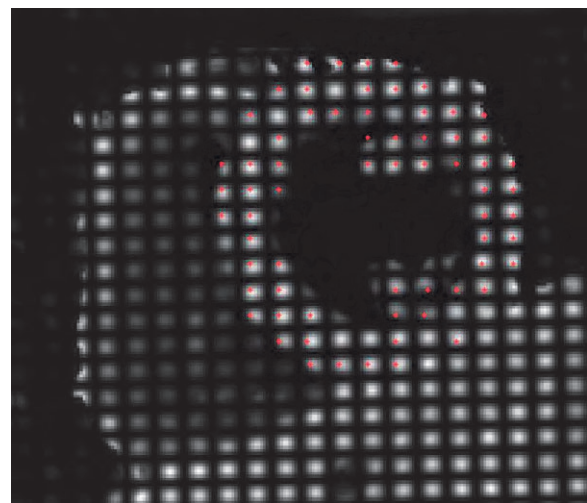


Fig. 1. Automatically selected control points in one frame of the simulated sequences.

with very good phase stability were chosen as control points. This automatic selection provides control points with robust tracking estimates that take into account prior information that is very valid for enhancing the method. In principle, it does not matter which points are selected, although it is desirable that they are evenly distributed, what is guaranteed by the automatic selection of the points in the tag intersections. It is also important to note that the computational time does not increase significantly, as only a few points are going to be selected. An example of a set of control points is shown in Fig. 1. Approximately, 60 control points are automatically selected in synthetic data (see Section 2.3.1) and around 40 control points in real data (see Section 2.3.2). This number is smaller for real sequences as the spatial resolution of these sequences is smaller, and there are less tag intersections in the myocardium.

### 2.3. Experiments

Two different experiments were performed, the first one with synthetic data and the second one with five different real datasets. The methods shown in the previous section have been compared both with a reference method (HARP) and with the manual tracking of structures.

#### 2.3.1. Experiments with synthetic data

The first experiments were conducted with synthetic data. The simulated sequence was generated from a real magnetic resonance CINE image with a pixel size of  $1.17 \times 1.17$  mm, a spatial resolution of  $176 \times 204$  pixels and a slice thickness of 8 mm [49]. The tags were simulated using a sinusoidal function in both directions.

The image has been deformed using a separable model in time and space using polar coordinates as follows

$$g_0(t, x) = \chi(r) \cdot \zeta(t) \quad (11)$$

where  $g_0$  is the image,  $\chi(r)$  represents the spatial deformation, and  $\zeta(t)$  simulates the left ventricular contraction through the cardiac cycle. The objective of the spatial deformation is to simulate the myocardial contraction, which causes more radial movement at the endocardium than at the epicardium. Therefore, the myocardial thickness changes when the temporal function is applied [49]. It is composed of a circumferential term that rotates the whole image to simulate circumferential movement of the heart, and it only depends on the distance of each point to the center of the ventricle.

$$\chi(r) = \left\{ \begin{array}{ll} k \cdot \sin\left(\frac{\pi r}{2 r_c}\right) & \text{for } r < r_c \\ k \cdot \sin\left(\frac{\pi}{2} \frac{r - r_1}{r_c - r_1}\right) & \text{for } r_c < r < r_{ext} \\ k \cdot \sin\left(\frac{\pi}{2} \frac{r_{ext} - r_1}{r_c - r_1}\right) & \text{for } r_{ext} < r \end{array} \right\} \quad (12)$$

where  $r_c$  is the endocardium radius,  $r_{ext}$  the pericardium radius and  $k$  a constant to change the amplitude of the displacement.

The equation of the temporal evolution function  $\zeta(t)$  is defined using a continuous pulse function  $\Pi(t_i, t_{i+1})$  in the range  $[t_i, t_{i+1}]$  based on hyperbolic tangents [34]:

$$\zeta(t) = \Pi(t_0, t_1) \cdot \sin^2\left(\frac{\pi \cdot t}{2 \cdot \frac{T}{3}}\right) + \Pi(t_1, t_2) \cdot (a + b \times t) \quad (13)$$

where  $t_0 = 0.0T$ ,  $t_1 = 0.446T$ ,  $t_2 = 0.960T$ ,  $a = 0.431$ ,  $b = -0.007$  and  $T = 33$

$$\Pi(t_i, t_{i+1}) = \frac{1}{4} (1 + \tanh(\alpha(t - t_i)))(1 + \tanh(\alpha(t_{i+1} - t))) \quad (14)$$

where  $\alpha = 1.136$ .

To run the experiments on these synthetic data, the myocardium was divided into six regions according to the standardized myocar-

dial division of segments [50]. In each region, four points were selected and tracked manually along each sequence. Overall, 24 points were selected along every sequence. Results obtained with the variational and the enhanced variational methods were compared with those obtained with HARP. The error for the three implementations was computed as a root mean squared (RMS) error.

The values of the parameters used in the program were selected experimentally by assigning different values to the parameters from given intervals and choosing the parameters which lead to a better convergence (fewer numbers of iterations) of the main equation (10). The parameter value intervals considered were  $\alpha^c \in (10^{-5}, 10^{-8})$ ,  $\alpha^r \in (10^{-5}, 10^{-7})$ , and  $\beta \in (10^{-5}, 10^{-7})$ . In this case, for the variational method the following values were chosen:  $\alpha^c = 10^{-7}$ ,  $\alpha^r = 10^{-5}$ . For the enhanced variational method, the parameters  $\alpha^c = 10^{-6}$ ,  $\alpha^r = 10^{-6}$  and  $\beta = 10^{-6}$  provided the best performance. The motion field was initialized by solving only the optical flow constraint equation (OFCE), term A of Eq. (3). To find the minimum of this term, we took its derivative with respect to  $v$  and set it to zero, clearing the terms  $v_1$  and  $v_2$ .

The same experiments were repeated with the same synthetic sequence and with four different levels of additive noise, with SNR of 34 dB, 26 dB, 23 dB and 20 dB. The noise has been added in the frequency domain. Real and imaginary parts of each image were computed, and a Gaussian distribution was added to each part independently. Results obtained with each technique in the noisy images were compared. In Fig. 2, two frames of the synthetic sequence corresponding to those without noise and with SNR = 34 dB are represented.

#### 2.3.2. Experiments with real data

The algorithms presented in Sections 2.1 and 2.2 were also tested with five real magnetic resonance sequences. Tagged MR images were acquired using an optimized tagging sequence on a Philips Intera 1.5 T (Philips Medical Systems, The Netherlands) and with a five-element phased-array coil dedicated to cardiac imaging [31]. The tagging sequence used was an enhanced version of the free breathing SPAMM sequence provided by the manufacturer of our Philips Intera scanner [45]. The proposed sequence makes use of Cartesian  $k$ -space filling, turbo gradient echo (GE) pulses and both ECG and respiration gating. The main parameters of the sequence are: matrix =  $192 \times 192$  (phase  $\times$  frequency), 4 NSA, rectangular FOV = 100%, acquisition percentage = 100%, TE = 1.9 ms, TR = shortest (5.5 ms for a heart rate of 80 bpm), flip angle =  $13^\circ$ , turbo factor = 8, slice thickness = 8 mm, orthogonal grid line spacing = 8 mm, respiratory synchronization = gating, acquisition time =  $1'12''$ , 13 phases for 80 bpm. With these parameters, the contrast between the marks and the tissue are enhanced and maintained until the last image of the dynamic series [45]. Five healthy volunteers were examined, and short axis images with a frame rate of 13 frames per cycle were acquired. Images were cropped to select the myocardial region of interest. Analyzed image sizes ranged from  $53 \times 53$  to  $165 \times 165$ .

Again, according to the standardized myocardial division of segments [50], the myocardium was divided into six regions, and four points of each region were manually tracked. Overall, 24 points were selected along each sequence. The points were selected at frame 0, which is the beginning of the systolic phase. Thus, at frame 0 the tracked points of all methods were identical but differed with increasing frame number. The experiments were performed using the variational method, the enhanced variational method and the reference method HARP. The results obtained with each method were compared with the displacements obtained from the points tracked manually. The error for the three implementations was computed as the average root mean square error for each segment.

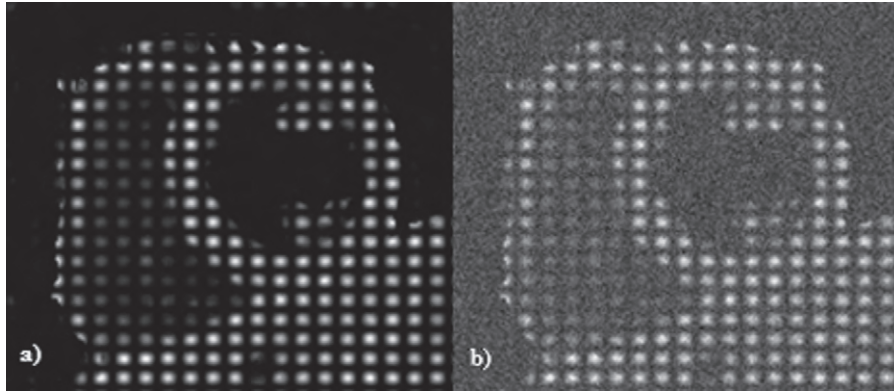


Fig. 2. (a) First image of the synthetic sequence without noise. (b) First images of the synthetic sequence with SNR = 34 dB.

The values of the parameters were set experimentally as described in Section 2.3.1 for the synthetic sequences by assigning different values within given intervals and choosing the parameters which lead to a better convergence behavior of the main Eq. (10). As a result, the values of the parameters used in the program were for the variational method:  $\alpha^c = 10^{-6}$  and  $\alpha^r = 10^{-7}$ . For the enhanced variational method, parameter values were  $\alpha^c = 10^{-8}$ ,  $\alpha^r = 10^{-7}$  and  $\beta = 10^{-7}$ . The best performance was obtained using these parameters, but we also tested the sensitivity of the results (difference in the average RMS error) performing the process using the same parameters used for the synthetic sequences. The motion field was initialized in the same way as explained for synthetic sequences.

To test if there is a statistically significant difference between the variational and the enhanced variational methods, a paired  $t$ -test was performed on the results obtained. Dependent samples (or “paired”)  $t$ -tests consist of a sample of matched pairs of similar units, or one group of units that has been tested twice (a “repeated measures”  $t$ -test). In our case, these are the tests performed with the variational method and enhanced variational method.

### 3. Results

#### 3.1. Results with simulated data

In Fig. 3, a comparison among the manually tracked points (triangles in blue color), the HARP method (circles in magenta color) and the enhanced variational method (diamonds in green color) is shown for one of the sequences. Three significant frames of the sequence are represented. In order to show the figures with more clarity, only one point per region has been shown. Note that blue triangles are barely distinguishable from the green diamonds due to the accuracy of the motion tracking.

From Fig. 3, it can be inferred that the results obtained with the enhanced variational method are very accurate and close to those tracked manually. Compared with the HARP method, our results are more stable and accurate, due to the tag jumping resulting from some of the points, which is an inherent drawback of this method.

The same simulated experiments were performed adding Gaussian noise with four different variances. The same reference points of the experiment shown above were used. The improvement achieved by the enhanced method is shown in Table 1. It shows the root mean squared error (in pixels) for the 24 points divided by the number of frames taken during the systolic phase. The improvement achieved can be inferred from these data.

As we can see in Table 1, results obtained by the enhanced variational method are closer to those obtained manually, and both the enhanced and original variational methods perform much better

than the original HARP technique. While the RMS error increases with the noise in the HARP method, the error decreases in the variational methods. This can be explained because the variational methods work better with smoother images. These variational methods can track points even in the presence of some noise due to the regularization term added.

To test if there is a statistically significant difference between the variational and the enhanced variational methods, a paired  $t$ -test was performed on these results. The  $p$  value obtained for a one-tail test of significance is 0.0022, which means that the difference is significant ( $p < 0.05$ ).

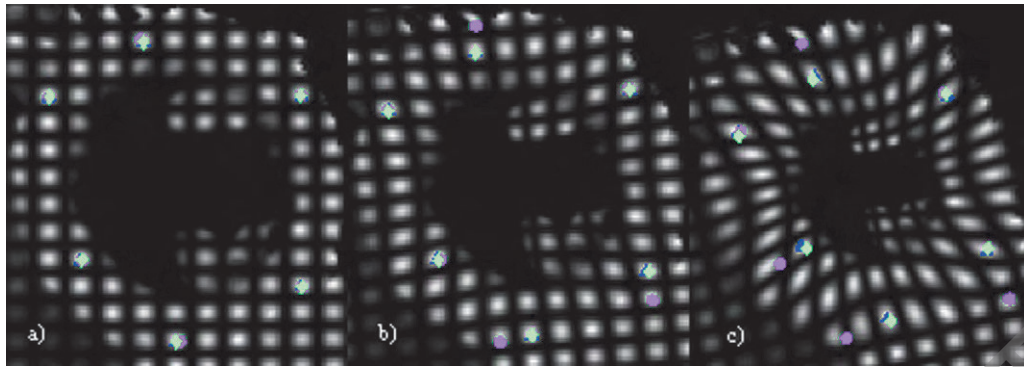
#### 3.2. Results with real data

Fig. 4 shows the optical flow recovered from one of the sequences on three illustrative frames. Blue triangles are the manually tracked points, magenta circles are the points obtained with the HARP method and the green diamonds are the points obtained by the enhanced variational method (the variational method has not been represented because the density of points was too high and the representation became confusing). Note that blue triangles are barely distinguishable from the green diamonds due to the accuracy of the motion tracking. In this picture, tag jumping of the HARP technique can be clearly observed. In spite of this, the enhanced variational method resulted in a good correlation with the manually tracked points along the whole sequence. The RMS error (in pixels) for all points in this sequence is 0.919 for the variational method, 0.802 for the enhanced variational method and 5.973 for the HARP technique.

When the parameters that resulted in the best performance for the synthetic sequences were used a very slight difference was obtained in the resultant error what actually corresponds to an averaged RMS error difference of 1.26%, corresponding to 0.0079 pixels.

To test if there is a statistically significant difference between the variational and the enhanced variational methods, a paired  $t$ -test was also performed on these results. The  $p$  value obtained for a one-tail test of significance is 0.0017, which means that the difference is significant ( $p < 0.05$ ).

Fig. 5a shows the average tracking RMS error for the five sequences tested using the variational method, the enhanced variational method, and HARP. For only the second sequence, the HARP method performed better than the variational method. But in that case, the enhanced variational method performed better than the others did. In all the other cases, the variational techniques performed much better than the HARP method. In Fig. 5b we can see the differences between the variational method and the variational enhanced methods for all the sequences. In all



**Fig. 3.** (a) First frame (b) fourth frame and (c) eighth frame of the sequence of the simulated data. Blue triangles are manually tracked points, magenta circles are the points obtained with the HARP method and the green diamonds are the points obtained by the variational method enhanced (For interpretation of the references to color in this figure legend, the reader is referred to the web version of the article).

**Table 1**  
Average RMS error for all the frame results obtained for the simulated data with and without noise.

RMS error (pixels)	Without noise	With noise			
		SNR = 34 dB	SNR = 26 dB	SNR = 23 dB	SNR = 20 dB
Variational method	0.611	0.595	0.565	0.518	0.448
Enhanced variational method	0.542	0.510	0.468	0.434	0.422
HARP method	4.924	5.373	5.449	5.364	5.610

cases, the enhanced variational method decreased the tracking error.

### 3.3. Computational cost

A study of the computational time required to run the implemented programs was conducted. The programs were written in MATLAB code and run in a PC with a 1.6 GHz Intel Pentium pro-

cessor with 1.23 GB RAM. In Table 2, results for the five sequences tested are shown.

As can be observed, the size of the sequences has been included in Table 2, since this factor influences the computational time. Comparing the computational time for the variational and enhanced methods, it can be seen that for the smaller sequences, the required time in the enhanced variational method is increased by two for sequence 5 and by two for sequence 1. Nevertheless, for sequences

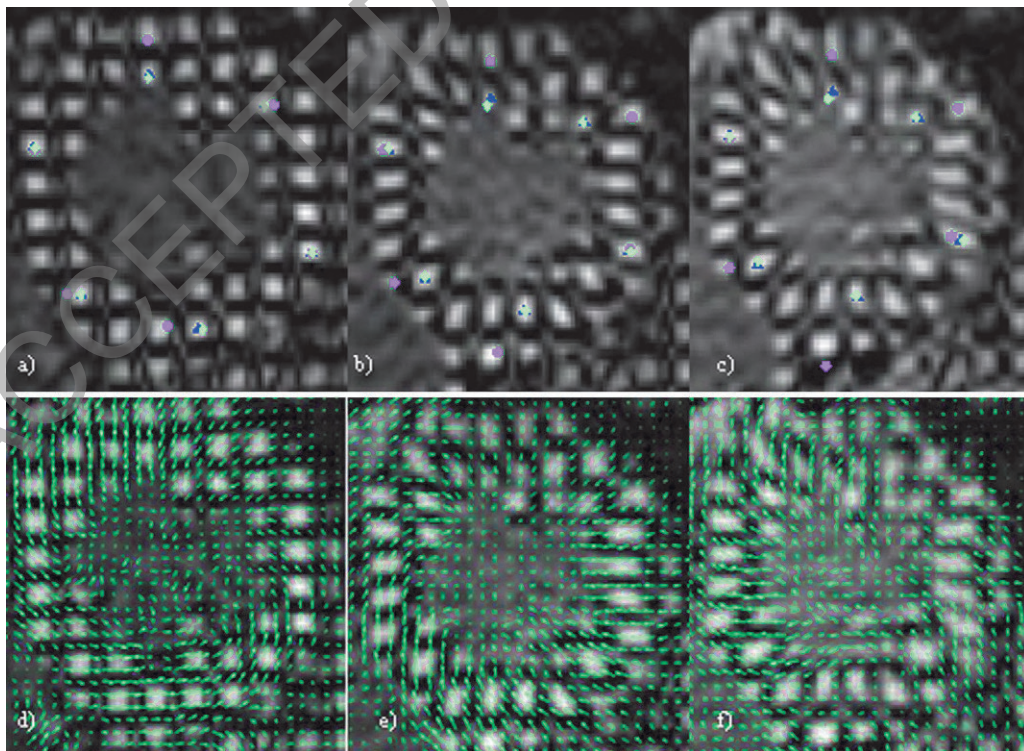


**Fig. 4.** (a) First frame (b) third frame and (c) fifth frame of the first real sequence. Blue triangles are manually tracked points, magenta circles are the points obtained with the HARP method and the green diamonds are the points obtained by the variational method enhanced. (d–f) Optical flow displacement fields for the same frames (For interpretation of the references to color in this figure legend, the reader is referred to the web version of the article).

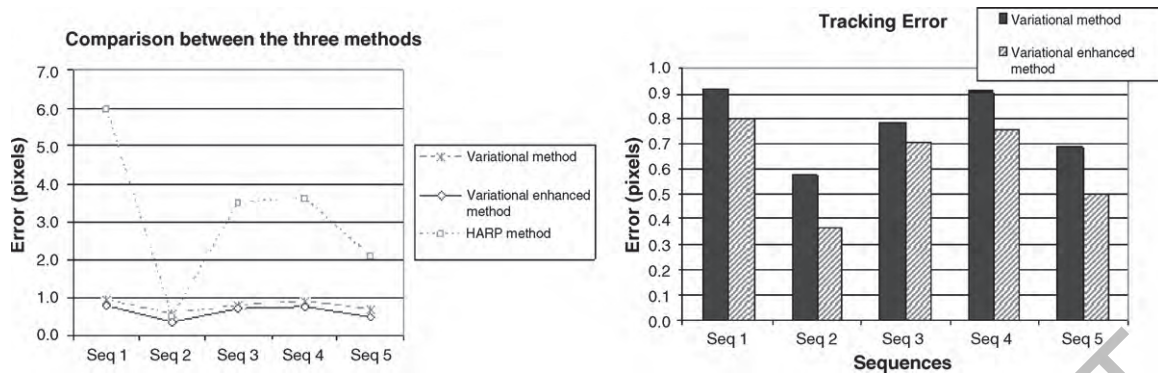


Fig. 5. (a) Comparison of the average tracking RMS error for the five sequences tested when the different methods, variational (asterisk), enhanced variational (diamond), and HARP (square) are used. (b) Average tracking RMS error for the five sequences tested with the variational (flat color) and enhanced variational (grated) method.

Table 2

Computational time obtained for the five sequences tested.

CASE		Computational time (s)			Ratio between computational time	
Seq	Size (pixels)	Variational method	Enhanced variational method	HARP, 24 points	Enh Var/Var	Enh. Var/HARP
1	123 × 110 × 7	19.518	108.857	52.14	5.518	2.088
2	65 × 63 × 7	13.329	49.982	10.44	3.150	4.187
3	165 × 165 × 7	182.232	223.973	102.287	1.229	2.190
4	126 × 126 × 7	43.623	72.915	64.233	1.621	1.135
5	53 × 53 × 7	5.628	11.356	10.947	2.018	1.037

with higher resolution (sequence 4 and 3), this time is increased by less than a factor of two. The computational time for including the control points becomes less relevant when the sequences are bigger. Evidently, the computational cost for the enhanced variational method will increase as long as we initially select more control points (this time is proportional to the number of control points selected). Nevertheless, it is important to achieve a reasonable compromise between computational cost and results obtained. In our implementation, we have initially selected one control point per tag, which appears to be a good result.

Regarding the HARP method, the computational time shown in Table 2 has been obtained only for the 24 points per sequence (the points tracked manually), which for the smallest sequence is less than 0.1% of the total amount of pixels of the image. It can be seen that in three out of the five sequences tested, the time obtained for computing only 24 points is higher than the time consumption of the variational method. That means that, for computing all the points of the sequence, the computational time will be much higher and not even comparable with the times obtained with variational methods. Comparing these results also with registration-based techniques for motion estimation [31], the computational cost is comparable to the enhanced variational method described here.

#### 4. Discussion and conclusions

In this paper, a new method for motion estimation for tagged cardiac magnetic resonance sequences has been presented. The technique is based on a variational approach that has been improved by taking into account the particular features of these types of images. Specifically, the variational method has been enhanced by tracking some selected points by means of their phase stability.

The new method has been tested with simulated data (with and without additive noise) and with real data. It has been compared with the HARP method and the standard variational method based on total variation. Results show that the variational method is more accurate than the HARP technique. Although results with HARP methods have been proved to be very accurate if the phase is reli-

able [10], in some cases large myocardial motion or image artifacts may cause points to be tracked to wrong locations (tag jumping) at a given time frame, causing erroneous tracking in successive frames as well. This fact has been confirmed by the numerous tests done in Section 3. On the other hand, comparing the results with other published works is difficult mainly because different data sets have been used, and the exact evaluation methodology is not thoroughly described or available. Taking into account this limitation, we can compare our results to those obtained by previously published methods [10,14,49,51] in terms of the RMS error reported in their validation experiments ranging from 0.3 pixels to 1.1 pixels. Therefore, the proposed method obtains comparable results in this sense taking advantage of all the inherent features of tagged sequences and requiring a low computational cost to compute the dense displacement field.

The enhanced variational method proposed provides superior results in most of the cases compared with the conventional variational method itself. Even if no control points are provided, the enhanced variational method will perform as well as the variational method. It has been proven that both methods are very robust to noise degradations of images, as is the case of the tagged cardiac magnetic resonance images. Even with a low temporal support (sometimes we have only six images in the systolic period), the proposed method is able to compute an accurate optical flow for each pair of images. The increase in the accuracy achieved with the enhanced variational method can be relevant in the presence of noise and for the computation of secondary parameters which involve spatial derivatives, such as the strain, which are effects that will be further investigated.

The proposed techniques could be useful in other applications as well, if some control points with confident motion estimation can be extracted. The computational cost of this enhancement is small, whereas the results are improved. In addition, with the variational method proposed, a dense optical flow is obtained for each sequence with a very small computational cost.

The major drawback of this method, and in general of all differential methods, comes with sequences with low temporal resolution, where the result of the temporal derivatives may not

be reliable. The temporal resolution could be decreased depending on the speed of the objects in the sequence. In the case of myocardial motion analysis from tagged cardiac magnetic resonance sequences systolic motion has been assessed accurately with the typically acquired temporal resolution. However, further investigation is guaranteed in whether these methods could be applied to early diastole assessment and the required temporal resolution required in that case. On the other hand, the selection of the parameters is not a trivial task. Further research will be focused on improving the method for parameter selection, with the aim of achieving the smallest possible motion estimation error. As it is known, one of the most prominent limitations of variational techniques is their dependence on the selection of parameters. In our experiments we noted a very slight difference in the results when the adjusted parameters for the synthetic sequences were used for the real data, however further analysis of this fact could be interesting regarding different MR scanners or acquisition protocols. On the other hand, it is important to note the advantages of variational techniques, such as their robustness to noise and the better tracking of point of interest.

### Acknowledgments

The authors thank Esther Pérez David and Manuel Desco, from the Hospital Gregorio Marañón for providing us with the CMR images. This research has been supported by the following grants from the Ministry of Science and Innovation: TEC2007-67025/TCM; TEC2006-28009-E, TIN2007-68048-C02-01, SINBAD (PS-010000-2008-1), the CDTI-CDTEAM project from the Spanish Ministry of Industry and with assistance from the European Regional Development Fund.

### References

- [1] Santos A, Ledesma-Carbayo MJ. Cardiac Imaging, vol.2. New Jersey: Wiley Encyclopedia of Biomedical Engineering, John Wiley & Sons Inc; 2006.
- [2] Clarysse P, Basset P, Khouas L, Croisille P, Friboulet D, Odet C, et al. Two-dimensional spatial and temporal displacement and deformation field fitting from cardiac magnetic resonance tagging. *Medical Image Analysis* 2000;4:253–68.
- [3] Götte MJW, van Rossum AC, Twisk JWR, Künjer JPA, Marcus JT, Visser CA. Quantification of regional contractile function after infarction: strain analysis superior to wall thickening analysis in discriminating infarct from remote myocardium. *Journal of American College of Cardiology* 2001;37:808–17.
- [4] Lieberman AN, Weiss JL, Jugdutt BI, Becker LC, Bulkley BH, Garrison JG, et al. Two-dimensional echocardiography and infarct size: relationship of regional wall motion and thickening to the extent of myocardial infarction in the dog. *Circulation* 1981;63:739–46.
- [5] Sinitsyn V. Magnetic resonance imaging in coronary heart disease. *European Journal of Radiology* 2001;38(3):191–9.
- [6] Billet F, Serresant M, Delingette H, Ayache N. Cardiac Motion Recovery by Coupling an Electromechanical Model and Cine-MRI Data: First Steps. *The MIDAS Journal – Computational Biomechanics for Medicine (MICCAI 2008 Workshop)* 2008.
- [7] Axel L, Montillo A, Kim D. Tagged magnetic resonance imaging of the heart: a survey. *Medical Image Analysis* 2005;9:376–93.
- [8] Mäkelä T, Clarysse P, Sipilä O, Pauna N, Pham QC, Katila T, et al. A review of cardiac image registration methods. *IEEE Transactions on Medical Imaging* 2002;9:1011–21.
- [9] Ozturk C, Derbyshire JA, McVeigh ER. Estimating motion from MRI data. *Proceedings of the IEEE* 2003;91(10):1627–48.
- [10] Osman NF, Kerwin WS, McVeigh ER, Prince JL. Cardiac motion tracking using CINE harmonic phase (HARP) magnetic resonance imaging. *Magnetic Resonance in Medicine* 1999;42:1048–60.
- [11] Aubert G, Deriche R, Kornprobst P. Computing optical flow via variational techniques. *Siam Journal on Applied Mathematics* 1999;60:156–82.
- [12] Aletas AH, Ingkanisorn WP, Mancini C, Arai AE. DENSE with SENSE. *Journal of Magnetic Resonance* 2005;176(1):99–106.
- [13] Gilliam AD, Epstein FH, Acton ST. Cardiac motion recovery via active trajectory field models. *IEEE Transactions on Information Technology in Biomedicine* 2009;13(2):226–35.
- [14] Deng X, Denney Jr TS. 3D myocardial strain reconstruction from tagged MR image data using a cylindrical B-spline model. *IEEE Transactions on Medical Imaging* 2004;23(7):609–12.
- [15] Bergvall E, Hedstrom E, Bloch KM, Arheden H, Sparr G. Spline-based cardiac motion tracking using velocity-encoded magnetic resonance imaging. *IEEE Transactions on Medical Imaging* 2008;27(8):1045–53.
- [16] Sampath S, Osman NF, Prince JL. A combined harmonic phase and strain-encoded pulse sequence for measuring three-dimensional strain. *Magnetic Resonance Imaging* 2009;27(1):55–61.
- [17] Osman NF, McVeigh ER, Prince JL. Imaging heart motion using harmonic phase MRI. *IEEE Transactions on Medical Imaging* 2000;19:186–202.
- [18] Guttman MA, Prince JL, McVeigh ER. Tag and contour-detection in tagged MR images of the left-ventricle. *IEEE Transactions on Medical Imaging* 1994;13:74–88.
- [19] Chen YS, Amini AA. A MAP framework for tag line detection in SPAMM data using Markov random fields on the B-spline solid. *IEEE Transactions on Medical Imaging* 2002;21(9):1110–22.
- [20] Young AA. Model tags: direct 3D tracking of heart wall motion from tagged MR images. *Medical Image Computing and Computer-Assisted Intervention – MICCAI'98* 1998;1496:92–101.
- [21] Quian Z, Montillo A, Metaxas D, Axel L. Segmenting cardiac MRI tagging lines using Gabor filter banks. *Engineering in Medicine and Biology Society 2003*. In: Proceedings of the 25th Annual International Conference of the IEEE, vol.1. 2003. p. 630–3.
- [22] Chen T, Wang X, Chung S, Metaxas D, Axel L. Automated 3D motion tracking using gabor filter bank. Robust point matching, and deformable models. *IEEE Transactions of Medical Imaging* 2009;14.
- [23] Kumar S, Goldof D. Automatic tracking of SPAMM grid and the estimation of deformation parameters from cardiac MR images. *IEEE Transactions on Medical Imaging* 1993;13:122–32.
- [24] Luo G, Heng PA. *IEEE Transactions on Information Technology in Biomedicine* 2005;9(3):430–46.
- [25] Young AA, Axel L. Three-dimensional motion and deformation of the heart wall: estimation with spatial modulation of magnetization – A model-based approach. *Radiology* 1992;185:241–7.
- [26] Denney T, Prince JL. Optimal brightness functions for optical flow estimation of deformable motion. *IEEE Transactions on Image Processing* 1994;3:178–91.
- [27] Gupta SN, Prince JL. On variable brightness optical flow for tagged MRI. *Information Processing in Medical Imaging* 1995:323–34.
- [28] Prince JL, Gupta SN, Osman NF. Bandpass optical flow for tagged MRI. *Medical Physics* 2000;27(1):108–18.
- [29] Dougherty L, Asmuth J, Blom A, Axel L, Kumar R. Validation of an optical flow method for tag displacement estimation. *IEEE Transactions on Medical Imaging* 1999;18:359–63.
- [30] Prince JL, McVeigh ER. Motion estimation from tagged MR image sequences. *IEEE Transactions on Medical Imaging* 1992;11:238–49.
- [31] Ledesma-Carbayo MJ, Derbyshire JA, Sampath S, Santos A, Desco M, McVeigh ER. Unsupervised estimation of myocardial displacement from tagged MR sequences using nonrigid registration. *Magnetic Resonance in Medicine* 2008;59:181–9.
- [32] Garot J, Bluemke D, Osman N, Rochitte C, McVeigh E, Zerhouni E, et al. Fast determination of regional myocardial strain fields from tagged cardiac images using harmonic phase (HARP) magnetic resonance imaging. *Circulation* 2000;98:1–8.
- [33] Pan L, Prince JL, Lima JA, Osman NF. Fast tracking of cardiac motion using 3D-HARP. *IEEE Transactions of Biomedical Engineering* 2005;52(8):1425–35.
- [34] Osman NF, Prince JL. Regenerating MR tagged images using harmonic phase (HARP) methods. *IEEE Transactions of Biomedical Engineering* 2004;51(8):1428–33.
- [35] Chambolle A, Lions PL. Image recovery via total variation minimization and related problems. *Numerische Mathematik* 1997;76:167–88.
- [36] Sroubek F, Flusser J. Multichannel blind deconvolution of spatially misaligned images. *IEEE Transactions on Image Processing* 2005;vol.14:874–83.
- [37] Sroubek F, Flusser J. Resolution enhancement via probabilistic deconvolution of multiple degraded images. *Pattern Recognition Letters* 2006;27:287–93.
- [38] Barron JL, Fleet DJ, Beauchemin SS. Performance of optical flow techniques. *International Journal of Computer Vision* 1994;12:43–77.
- [39] Orkisz M, Clarysse P. Estimation du flot optique en présence de discontinuités: une revue. *Traitement du Signal* 1996;13:589–613.
- [40] Carranza N, Cristóbal G, Santos A, Ledesma-Carbayo MJ. Motion estimation and segmentation of cardiac magnetic resonance images using variational and level set techniques. In: Proceedings of the 16th European Signal Processing Conference 2008. 2008.
- [41] Horn BKP, Schunck BG. Determining optical flow. *Artificial Intelligence* 1992;17:185–203.
- [42] Aubert G, Kornprobst P. *Mathematical Problems in Image Processing. Partial Differential Equations and the Calculus of Variations*. Springer; 2006.
- [43] Deriche R, Kornprobst P, Aubert G. Optical flow estimation while preserving its discontinuities: a variational approach. In: Invited Session Papers from the Second Asian Conference on Computer Vision: Recent Developments in Computer Vision, vol. 1035. 1995. p. 71–80.
- [44] Charbonnier P, BlancFeraud L, Aubert G, Barlaud M. Deterministic edge-preserving regularization in computed imaging. *IEEE Transactions on Image Processing* 1997;6:298–311.
- [45] Santa-Marta C, Ledesma-Carbayo MJ, Bajo A, Pérez-David E, Santos A, Desco M. Respiratory Gated SPAMM Sequence for Magnetic Resonance Cardiac Tagging. *Computers in Cardiology, Valencia (Spain)* 2006.
- [46] Zerhouni EA, Parish DM, Rogers WJ, Yang A, Shapiro EP. Human heart: tagging with MR imaging—a method for non-invasive assessment of myocardial motion. *Radiology* 1988;169:59–63.

- [47] Axel L, Dougherty L. MR imaging of motion with spatial modulation of magnetization. *Radiology* 1989;171:841–5.
- [48] Axel L, Dougherty L. Heart wall motion: improved method of spatial modulation of magnetization for MR imaging. *Radiology* 1989;172:349–50.
- [49] Ledesma-Carbayo MJ, Kybic J, Desco M, Santos A, Suhling M, Hunziker P, et al. Spatio-temporal nonrigid registration for ultrasound cardiac motion estimation. *IEEE Transactions on Medical Imaging* 2005;24:1113–26.
- [50] Cerqueira MD, Weissman NJ, Dilsizian V, Jacobs AK, Kaul S, Laskey WK, et al. Standardized myocardial segmentation and nomenclature for tomographic imaging of the heart: a statement for healthcare professionals from the cardiac imaging committee of the council on clinical cardiology of the American heart association. *Journal of the American Heart Association* 2002;105:539–42.
- [51] Chandrashekhara R, Mohiaddin RH, Rueckert D. Analysis of 3D myocardial motion in tagged MR images using nonrigid image registration. *IEEE Transactions on Medical Imaging* 2004;23:1245–50.

**Noemí Carranza-Herrezuelo** was born in Valladolid, Spain, in 1980. She received her Ph.D. from the Polytechnic University of Madrid in 2009. She has worked in the Institute of Optics (CSIC) in the field of medical imaging processing during her predoctoral work. Her research interests include biomedical imaging and telemedicine.

**Ana Bajo** was born in Madrid (Spain) in 1981. She got her MSC Degree in Telecommunications Engineering in 2005, in the Technical University of Madrid (Universidad Politécnica de Madrid). She joined the Biomedical Image Technology Lab (BIT-UPM) in October 2004 to develop her Master Thesis. Since 2005 she is Research Fellow of the Biomedical Image Technology Lab (BIT-UPM), where she is currently doing her PhD in the field of medical image processing, specifically working in cardiac motion estimation with magnetic resonance imaging in collaboration with the Hospital Gregorio Marañón (HGGM), Madrid, Spain and the National Institutes of Health, Bethesda, Maryland, USA.

**Filip Sroubek** received the Ph.D. degree in computer science from the Charles University, Prague, Czech Republic in 2003. From 2004 to 2006, he was on a postdoctoral position in the Instituto de Optica, CSIC, Madrid, Spain. Currently, he is with the Institute of Information Theory and Automation, Academy of Sciences of the Czech Republic, Prague. He is an author of 4 book chapters and over 40 journal and conference papers on image fusion, blind deconvolution, super-resolution, and related topics.

**Cristina Santamarta** was born in León, Spain, in 1966. She graduated in Physics at the Universidad Complutense de Madrid in 1990 and received her PhD from the Universidad Politécnica de Madrid in 2004. She has been working for Philips Medical Systems as an MR applications specialist for six years while doing her thesis research. Now she works as assistant professor at the Universidad Nacional de Educación a

Distancia in Madrid. Her research interest is on sequence developing and image processing in the MR imaging field.

**Gabriel Cristobal** received the MSc and PhD degrees both in telecommunication engineering from the Polytechnic University of Madrid, Spain, in 1979 and 1986 respectively. He is currently a Research Scientist at the Instituto de Optica, Spanish Council for Scientific Research (CSIC). He was a Postdoctoral Fellow at the International Computer Science Institute and the Electronic Research Lab (UC Berkeley) from 1989 to 1992. His current research interests are joint representations, vision modelling and multidimensional signal processing. He has published more than 80 papers in technical journals and conferences. He has been responsible for several national and EU research and development projects. He is a Senior Member of the IEEE, OSA and SEDOPT member and EURASIP spanish liaison for the period 2009–2010. He is a member (and head of the Spanish delegation) of the ISO/IEC/SC29/WG01 JPEG 2000 Committee, since 2000.

**Andres Santos** was born in Valencia (Spain) in 1958. He has a M.Eng and a Ph.D. from Universidad Politécnica Madrid, where he is Professor in the Electronics Engineering Department during 1987–1988 he was International Research Fellow at SRI International (Menlo Park, California). His main areas of expertise are related to biomedical engineering, mainly biomedical image acquisition and processing. He has been co-director of a Master in Biomedical Engineering and since 1995 he also teaches biomedical signal processing in the ERASMUS/TEMPUS European Course on Biomedical Engineering and Medical Physics (University Patras – Greece). Currently he is the director of the Biomedical Imaging Technologies Lab., a research group oriented to developing new technologies for biomedical image acquisition, processing and analysis. Coordinator of several national and international projects on biomedical imaging and author or co-author of more than 150 international publications.

**María J. Ledesma-Carbayo** graduated in telecommunication engineering in 1998, with a master thesis on medical image analysis. Previously, in 1997/1998, she followed the ERASMUS European Course on Biomedical Engineering and Medical Physics in University Patras (Greece). She is now associate professor in the Electronics Engineering Department (Universidad Politécnica de Madrid), and she has obtained her PhD degree in biomedical imaging several years ago. She has visited for several months the Medical Vision Lab. at Oxford University in 1999, École Polytechnique Fédéral in Lausanne, in 2000 and 2001, and recently she has spent six months on the Cardiac Energetics Lab. at the National Institutes of Health (USA). Her main research areas of interest are medical image analysis and processing, especially those topics dealing with registration, cardiac imaging and motion estimation and compensation. Her research in medical imaging processing has been published in journals and conferences (more than 50). She has a lot of experience participating in research projects, from the Spanish Financial Offices, International Agencies and International Companies. Member of IEEE.